

Research Paper

Cite this article: Amin F, Raman S, Koh K-J (2018). Tunable Q-enhanced LC dual-band filtering at microwave frequencies in 0.13 μm SiGe BiCMOS. *International Journal of Microwave and Wireless Technologies* **10**, 635–642. <https://doi.org/10.1017/S1759078718000429>

Received: 1 September 2017

Revised: 12 February 2018

Accepted: 18 February 2018

First published online: 17 April 2018

Keywords:

Active circuits; filters; integrated tunable dual-band filter

Author for correspondence: Farooq Amin,

E-mail: famin@vt.edu

Tunable Q-enhanced LC dual-band filtering at microwave frequencies in 0.13 μm SiGe BiCMOS

Farooq Amin, Sanjay Raman and Kwang-Jin Koh

Bradley Department of Electrical and Computer Engineering, Virginia Polytechnic Institute and State University, Blacksburg, VA 24061, USA

Abstract

This paper presents an active Q-enhanced LC dual-band band-pass filtering approach using parallel synthesis techniques at X- and Ku-bands in 0.13 μm SiGe BiCMOS technology. By employing two independently tunable parallel LC-tanks with either in-phase and out-of-phase addition, independently tunable dual-band filtering is achieved. For higher out-of-band (OOB) attenuation, subtraction of the two 2nd-order bandpass filter is implemented. The two bands are independently tunable in terms of Q and center frequency. The dual-band filter at 9.7 GHz and 13.9 GHz achieves a normalized dynamic range of 165–154.5 dB.Hz with an OOB attenuation of >50 dB below 3 GHz. In between the two bands, the attenuation is 22 dB when the two passbands have 200 MHz bandwidth each. The total group delay is 0.8 ns and 1.9 ns for Q of 20 and 50, respectively. The filter achieves better OOB rejection with wider band channels at X- and Ku-bands compared with state of the art integrated filters. The filter consumes 115–130 mW of DC power. The core die area is $0.53 \times 0.7 \text{ mm}^2$.

Introduction

Modern wireless communication and radar systems require multi-purpose, multi-standard, and multi-frequency radio frequency (RF) front-ends that can operate in the presence of strong interference. This requirement is due to rapid increase of various systems, standards, and co-existing in the same spectrum. As a result there is a significant interest in multi-band band-pass filters (BPF), particularly dual-band filters. Additionally, future communication systems are shifting towards higher-frequencies, in the range of microwave to millimeter-wave. Conventionally, dual-band filters in the microwave regime have been designed using substrate integrated waveguide (SIW) cavities and/or microstrip lines [1–7] which are not practical to integrate on chip. These solutions also typically lack tuning capabilities, and therefore, multiple switched filters are needed to cover different frequency bands. The cost and form factor of such solution thereby increases significantly. Numerous off-chip techniques to obtain dual-band response have been proposed in [1,3–7] including stepped impedance resonator, capacitively loaded dual cavity resonators, and microstrip-based coupled resonating sections. An off-chip passive tunable multiband BPF covering 0.8–1.2 GHz, employing Wilkinson type power divider [2], has been reported with good performance but with limited integration capability and large area. To date, no work has been reported for on-chip dual-band operation at higher microwave frequencies. For cost effective multiband systems, one practical solution is to use minimal off-chip bulky filters with a wide pass-band coverage, in conjunction with on-chip tunable filter to reject the out-of-band (OOB) interferers further.

Recent developments in on-chip filtering include N-path and Q-enhanced LC filters [8–12]. N-path filters typically employ a wideband low-noise amplifier followed by a narrowband frequency tunable filtering [8,10–12] using switches driven by N no. of multi-phase clocks. These filters, however, are mostly limited to lower RF frequencies (below ~ 3 GHz) and their filtering performance degrades as frequency increases. This degradation is due to switch parasitics which limit the OOB attenuation as well as inaccurate multi-phase clock generation at higher frequencies with associated large power consumption. For example in [7], at the expense of significant power consumption, the OOB attenuation is still limited to 20 dB or worse at frequencies above 10 GHz in CMOS SOI 32 nm.

Compared with N-path filters, Q-enhanced LC filtering is quite suitable at higher microwave frequencies due to increased on-chip inductor Qs and reduced size [9,13]. Additionally Q-enhanced LC filtering provides increased OOB attenuation, and potential for fast frequency tuning.

In this paper, an on-chip Q-enhanced dual-band filtering solution based on prior work single-band tunable designs is presented along with measured results at microwave frequencies. The section “Synthetic parallel dual-Band filtering” introduces the parallel synthesis technique and analysis. The section “Circuit design and implementation” covers detailed

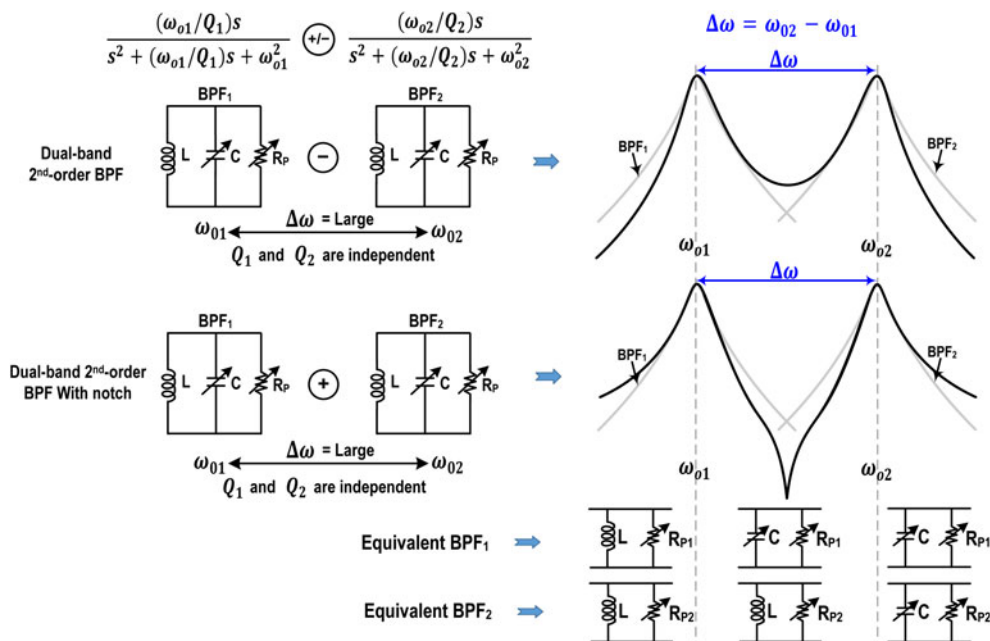


Fig. 1. Shaping of dual-bands BPF responses by parallel synthesis of two tunable (Q and center-frequency) LC-tanks.

implementation followed by measurement results in the section “Measurement results”. Finally, the section “Conclusion” concludes this work.

Synthetic parallel dual-band filtering

Figure 1 shows the concept of parallel synthesis techniques using two LC-tanks. The center frequencies of the LC-tanks are tunable using the varactors C. The Q of the LC-tank can be tuned using a variable load resistance R_p . By exploiting the LC-tank’s phase characteristics, two types of dual-band band-pass shaping are achievable. The first characteristic is achieved by subtracting the two LC-tank responses with largely spaced center frequencies ω_{01} and ω_{02} to form a dual-band filter response with higher OOB attenuations. However, between bands the attenuation is 6 dB less compared with the 2nd-order BPF responses alone. This can be explained by the phase changes of the two LC-tanks where both LC-tanks are inductive below the center frequency ω_{01} of BPF₁ and therefore, are in phase. When the responses are subtracted in this region the resulting roll-off will be steeper than the 2nd BPFs alone. The same is true for the region higher than the center frequency ω_{02} of BPF₂. In between the two center frequencies ω_{01} and ω_{02} , BPF₁ is capacitive whereas BPF₂ is inductive; hence, they are out-of-phase resulting in addition of the waveforms when the outputs are subtracted. The second characteristic is achieved by adding the two LC-tank responses. This results in a sharp notch between the two center frequencies for higher attenuation between the bands. However, the ultimate rejection levels on the higher and lower sides of the center frequency worsen by 6 dB compared with individual 2nd-order BPF responses due to additive common impedance by the two BPFs. The choice of addition or subtraction to form dual-band responses depends on the application and operating frequencies; nevertheless, a trade-off exists between in-band attenuation versus OOB attenuation. The addition mode resulting in the deeper notch may be desirable at lower RF frequencies where an attenuation in-between the bands is important. The

subtraction mode is favorable, in general, at higher microwave frequencies where the band separations are larger. To find the attenuation in-between bands, the 2nd-order transfer function can be expressed as

$$H(s) = \frac{\frac{\omega_0}{Q}s}{s^2 + \frac{\omega_0}{Q}s + \omega_0^2} \tag{1}$$

$$H(s = j\omega) = \frac{1}{1 + jQ\left(\frac{\omega}{\omega_0} - \frac{\omega_0}{\omega}\right)}, \tag{2}$$

for large Q, (2) can be expressed as

$$|H(j\omega)| \approx \frac{1}{Q\left(\frac{\omega}{\omega_0} - \frac{\omega_0}{\omega}\right)}. \tag{3}$$

To find attenuation between bands by the first BPF, substitute $\omega_0 = \omega_{01}$ and $\omega = \omega_{01} + \frac{\Delta\omega}{2}$, and after approximation, (3) can be expressed as

$$|H(j\omega)| \approx \frac{1}{2Q} \cdot \left(\frac{\omega_{02} + \omega_{01}}{\omega_{02} - \omega_{01}}\right). \tag{4}$$

Therefore, for the same Q of each band, the total attenuation between bands will be added and can be expressed in dB as

$$A_T = 20 \log\left(\frac{1}{2Q} \cdot \frac{(\omega_{02} + \omega_{01})}{(\omega_{02} - \omega_{01})}\right) + 6(dB), \tag{5}$$

where ω_{01} and ω_{02} are the center frequencies of LC-tanks. This shows that the in-between bands attenuation is degraded by 6 dB compared with a 2nd-order BPF response.

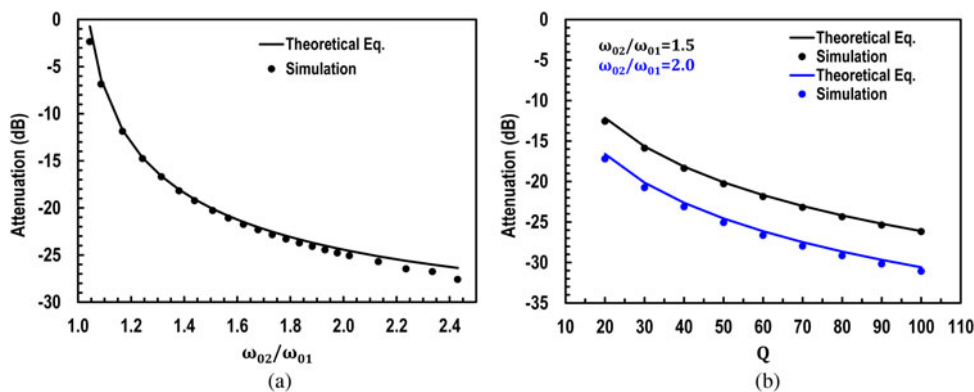


Fig. 2. (a) In-between bands attenuation for theoretical approximate equation and simulation (a) versus dual-band frequencies ratio and (b) versus Q of the each dual bands.

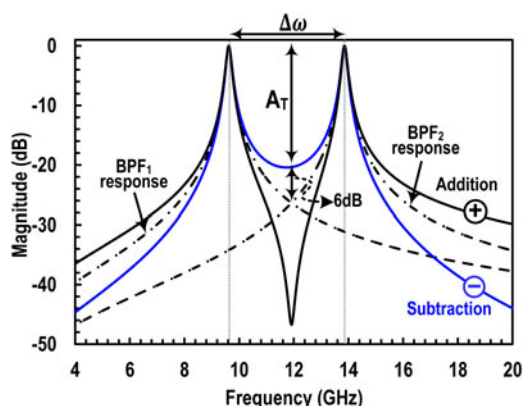


Fig. 3. Ideal lumped circuit simulations of dual-band BPF at 9.7 and 13.9 GHz.

Figure 2(a) shows the simulation and the approximate relation derived in (5) against the frequency spacing between the two bands in terms of ratio of $\omega_{02}-\omega_{01}$. In this case, the Q of each BPF is 50 and the spacing between the two bands are varied from very small to when ω_{02} is twice that of ω_{01} . The plots shows agreement between the simulation and the theoretical approximation. The relation in (5) can reveal important design parameters in terms of Q and spacing between the two bands to achieve a targeted attenuation. For example, when Q of both bands is set to 50, the spacing resulting in $\omega_{02} = 1.5\omega_{01}$ guarantees at least 20 dB of attenuation.

Figure 2(b) shows the plots of theoretical equation and simulation versus Q of the two bands for two cases of ω_{02} and ω_{01} spacing. For the Q of 100 of each band, the attenuation is more than 31 dB when ω_{02} is twice that of ω_{01} . An ideal lumped components simulation with dual-bands around 10 and 14 GHz each having 200 MHz of bandwidth (BW) is shown in Fig. 3. The trade-off between in-between bands and OOB attenuation is evident for the two synthesis cases of addition and subtraction. Note the OOB attenuation on higher side of the 14 GHz for the case of subtraction compared with addition, thus mitigating the effects of less roll-off of BPF. As proof of concept of this approach, the subtraction mode was demonstrated using the design of [13].

Circuit design and implementation

The proposed parallel synthesis techniques requires independent tuning of the center frequency and Q of the LC-tanks. Figure 4

(a) shows the block diagram of the proposed filter where two tunable 2nd-order BPFs outputs are subtracted using transistors (Q_{A-B}) and (Q_{C-D}) and resistor R_0 and R_E . Resistance R_0 also serves to match to 50 Ω output for measurement purposes.

2nd-order BPF tuning

The LC-tanks are driven by a buffer and a transconductor as shown in Fig. 4(a) for voltage and current mode driving, respectively. Since the LC-tanks are driven as well as loaded by active components, no coupling exists between the two resonators, contrary to the case of traditional all-passive ladder and coupled resonator filter structures. Hence, the two LC-tanks can be independently controlled in terms of Q and center frequency tuning. The input buffer, realized by $Q_{1,2}$ (Fig. 4(b)), drives the LC-tank in voltage mode. The variable resistor R_C consists of an nMOS M_1 and a resistor (Fig. 4(c)) which is used to reduce the Q to as low as 4. A variable transconductance G_m , realized by Q_3 together with variable resistance R_G and M_2 in parallel (Fig. 4(d)) is used to drive the tank in current mode in order to control the gain of the LC-tank. This enables control of the trade-off between noise and linearity. The LC-tank losses R_P are compensated by a Darlington-type negative resistance R_N as shown in Figure 4(e). This consists of a fixed negative $1/G_m$ realized by $Q_{5,6}$ and R_Y and a variable negative $1/G_m$ realized using nMOS $M_{3,4}$ and resistance R_X . The Q can be increased to more than 100 by controlling the negative resistance using $M_{3,4}$. This control also helps in keeping each BPF path stable.

The proposed dual-band band-pass filter, Fig. 4, is implemented in IBM 0.13 μm SiGe BiCMOS process with $f_T/f_{max} = 180/220$ GHz. The fabricated chip photograph is shown in Fig. 5. Great efforts were made to achieve highly symmetric layout for differential matching. The core size of the filter, excluding pads, occupies $0.53 \times 0.7 \text{ mm}^2$. The total chip area is $1.05 \times 0.95 \text{ mm}^2$.

2nd-order BPF Q and stability

On-chip spiral inductors typically have low Q due to the sheet resistance of the inductor metal traces, substrate losses, and the skin effect; these losses can be modeled as a series resistance which must subsequently be mitigated using Q -enhancement.

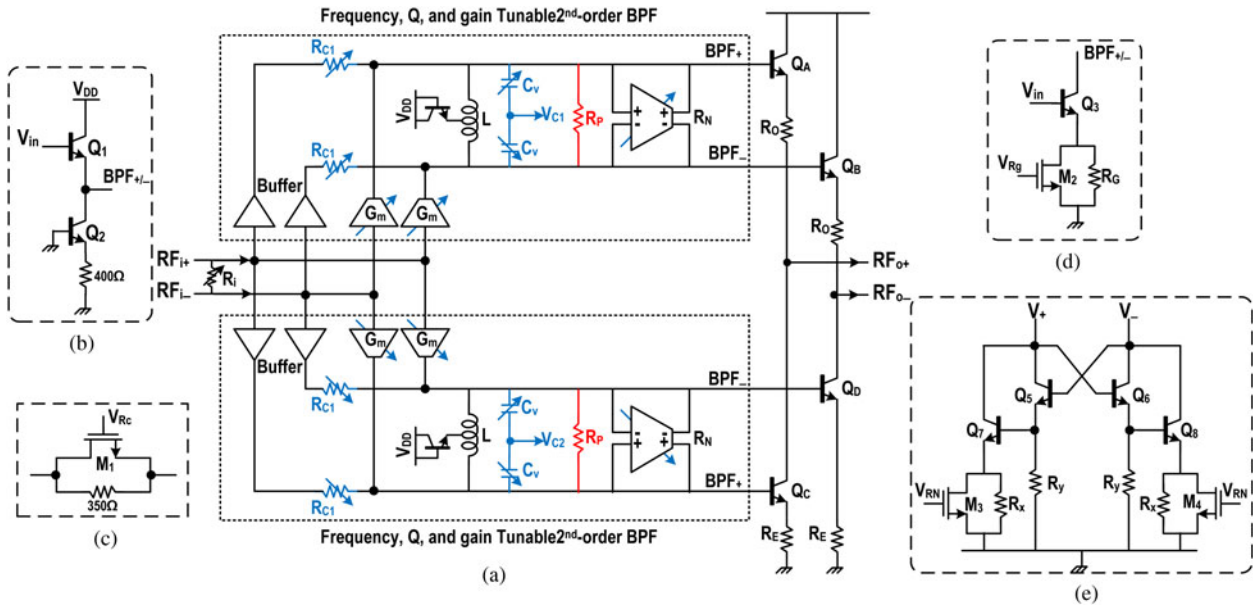


Fig. 4. (a) Schematics diagram of the proposed filter using two 2nd-order BPFs with independent tuning, (b) the buffer cell, (c) the resistance R_{C1} implementation, (d) the variable G_m cell, and (e) a linearized variable negative resistance R_N implementation.

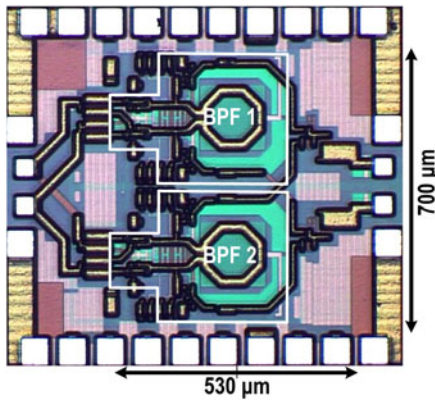


Fig. 5. IBM SiGe 130 nm chip micrograph with core area of $0.7 \times 0.53 \text{ mm}^2$.

The 2nd-order LC BPF consists of one parallel resonator or tank, which provides two-negative frequency poles. For a lossy on-chip inductor the effective tank Q is that of the inductor with loss R_S at the resonance frequency of the tank: $Q_0 = \frac{\omega_0 L}{R_S} = \frac{1}{R_S} \sqrt{\frac{L}{C}}$. Then the equivalent parallel inductor L_P and loss R_P can be written as

$$L_P = \left(\frac{1 + Q_0^2}{Q_0^2} \right) L_S, \quad R_P = (1 + Q_0^2) R_S \approx \frac{\omega_0^2 L^2}{R_S}. \quad (6)$$

A negative resistance $R_N = -1/G_m$, to cancel the equivalent parallel loss R_P , can be implemented using a transconductor with positive feedback as shown in Fig. 4(e). The equivalent parallel resistance R_{EQ} and the enhanced quality factor Q_{EN} can be expressed as

$$R_{EQ} = R_P \parallel \left(-\frac{1}{G_m} \right) = \frac{R_P}{1 - G_m R_P}, \quad (7)$$

$$\text{and } Q_{EQ} = \frac{R_{EQ}}{\omega_0 L_P} = \frac{Q_0}{1 - G_m R_P}. \quad (8)$$

The Q can be made very high when $G_m R_P \rightarrow 1$. However, the $-G_m$ needs to be precisely controlled to avoid oscillation which happens when the equivalent resistance R_{EQ} becomes negative. i.e. $G_m R_P \geq 1$.

Fig. 6(a) shows the Q of the LC-tank before compensation and the total tank Q with a load resistance $R_C = 350\Omega$. The inductor Q , based on electromagnetic simulations, varies from 13~18 for frequencies 8~15 GHz whereas the varactor Q varies from 30~115. The resultant LC-tank Q with a load resistance $R_C = 350\Omega$ is in the range of 9~10 including all parasitic effects from interconnects. With compensation by the negative resistance R_N for both tanks, the Q can be increased to 100 or more. Fig. 6(b) shows the post-layout stability simulations of the proposed filter as well as the measured stability factor from S-parameters. The simulation results show that for a Q of 100 for both bands, the stability parameters $K_2 > 1$ and $B1_2 > 0$ are satisfied by a large margin guaranteeing that the filter is unconditionally stable over large frequency range. The measured stability parameters are also plotted for $Q = 67$ from 1 to 22 GHz showing unconditional stability similar to simulations.

Measurement results

To verify the proposed tunable dual-band filter approach, the fabricated chip was measured using GSSG probes with differential SOLT calibration. To interface with single-ended 50Ω equipment, 180° hybrid couplers were used for differential to single-ended conversion. The measured dual-band filter response is plotted in Fig. 7(a) which shows normalized S_{21} plots for different Q s, ranging from 20 to 67. The Q tuning is independent and continuous by controlling each tank's R_C and R_N (Fig. 4(a)) though only discrete Q tuning steps are shown for clarity. The dual-bands are

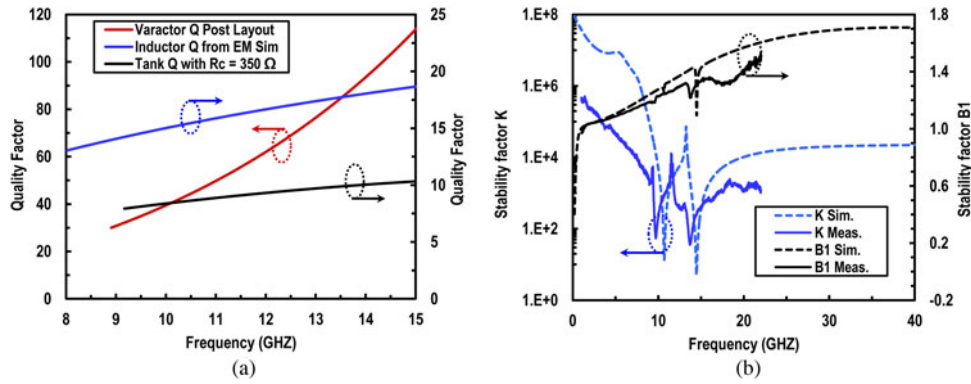


Fig. 6. (a) Post layout simulated Q of the LC-tank components and (b) simulated stability factors when Q is increased to 100 using negative gm and measured stability factors for Q = 67.

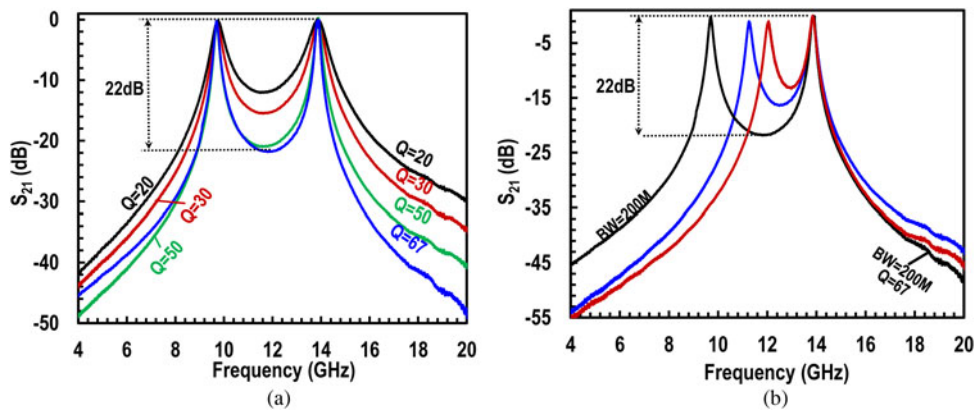


Fig. 7. (a) Measured filter response at 9.7 and 13.9 GHz with Q tuning from 20 to 50 and (b) measured center frequency tuning.

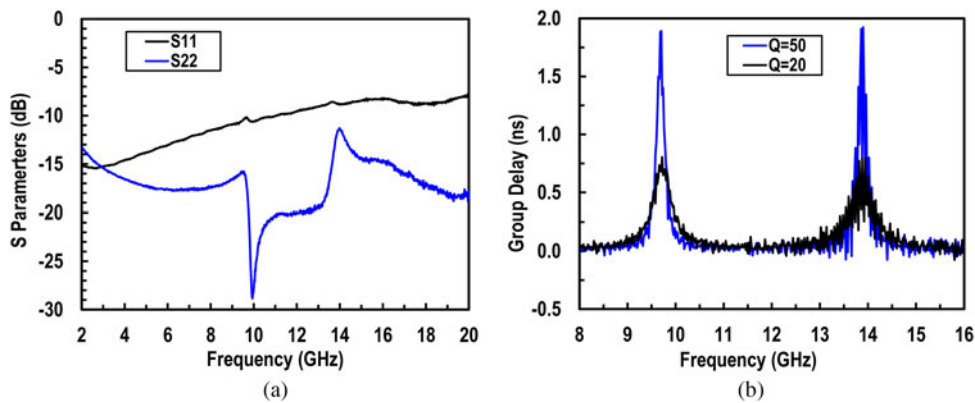


Fig. 8. Measured (a) S_{11} and S_{22} and (b) group delay for Q of 20 and 50.

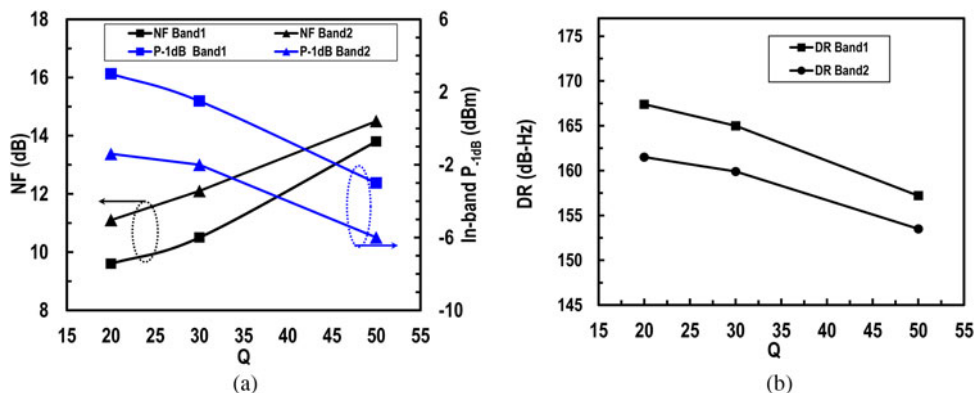


Fig. 9. Measured (a) in-band input P_{-1dB} and noise figure (NF) versus Q and (b) normalized dynamic range.

tuned at 9.7 and 13.9 GHz. With this band-separation, the attenuation is more than 22 dB for BW of 200 MHz each. Due to subtraction, the OOB attenuation on the lower side is > 50 dB below 4 GHz, and, more significantly, > 48 dB on the higher side of the filter at 20 GHz and above. The roll off continues on the lower and upper side frequencies beyond the plot limits. The bands can be tuned independently up and down in frequency using varactor control, while Fig. 7(b) shows the band tuning across the frequency by tuning the lower BPF.

The S_{11} and S_{22} measurements are shown in Fig. 8(a) for the filter tuned at 9.7 and 13.9 GHz. each with Q of 50. The output matching is very good with $S_{22} < -14$ dB. The S_{11} is -10.2 and -8.8 dB at 9.7 and 13.9 GHz, respectively. The group delay measurement plots are shown in Fig. 8(b) for Q s of 20 and 50. The total group delay is around 0.8 ns for $Q=20$ and 1.9 ns for $Q=50$. The noise figure (NF) and input P_{-1dB} are plotted in Fig. 9(a). The NF is measured for both input matched and high impedance case using R_i in Fig. 4 (a). The normalized dynamic range (DR), the ratio of input P_{-1dB} to the 1-Hz BW input referred noise, for the input matched case is plotted in Fig. 9(b). The normalized DR varies from 164.6 ~ 154.5 for the lower band, and 160~152 for the upper band for $Q=20 \sim 50$ at the expense of 115-130 mW DC power. The measured input P_{-1dB} for $Q=20 \sim 50$ is 3~-3.6 dBm and -1~-6 dBm for lower and upper bands, respectively. The NF can be reduced by increasing the gain from the variable transconductance amplifier G_m in Fig. 4(a).

Table 1 shows the performance summary and comparison with state of the art on-chip dual-band filters. The proposed Q -enhanced dual-band filtering is advantageous at microwave frequencies with higher OOB attenuation, independent dual-band tuning, and better DR performance compared with prior integrated N-path filters implementation. Additionally the proposed dual-band filter performance is also compared with off-chip filters in Table 2. The off-chip filters are generally higher-order than this work's 2nd dual-bands. It is also worth mentioning that most of the off-chip filters have dual-band center frequency ratios of more than 2. Apart from small area and flexible tunability, the proposed filter, if designed for frequency ratios > 2, can achieve in-between bands attenuation, as shown in Fig. 2(b), similar to off-chip filters in Table 2.

Conclusion

This paper demonstrated an integrated Q -enhanced dual-band filtering solution at X- and Ku-band microwave frequencies using 0.13 μm SiGe BiCMOS. The concept of dual-band independent tuning operation can be extended to wide range of operating frequencies by appropriately designing the tanks. The filter DR is 164.6–154.5 dB and 160–152 dB at the demonstrated lower (9.7 GHz) and upper (13.9 GHz) bands, respectively. The dual-band filtering approach using the subtraction method has the advantage of increased OOB attenuation on the lower and upper sides of the two passband responses. Future work includes integration of a selection mechanism using switches to provide both subtraction and addition modes on demand depending on system or operational requirements.

Acknowledgments. This work was partially supported by BAE Systems MICS Industry Affiliates Program membership and the Virginia Space Grant graduate fellowship. The silicon chip fabrication was supported by DARPA.

Table 1. Performance comparison with on-chip filters

References	Type	Freq. (GHz)	Channels/Bands	BW of each Band (MHz)	Filter Q	NF (dB)	IP _{-1dB} (dBm)	Normalized DR ^c (dB-Hz)	Ultimate Rejection (dB)	Power (mW)	Area (mm ²)	Process
This Work	Q-enhanced LC	9.7 ~ 13.9	2	200 ~ 700	20 ~ 67	9.6 ~ 13.8 ^d	-3 ~ 3.6 ^d	165 ~ 154.5 ^d	> 50	115 ~ 130	0.371	130 nm SiGe BiCMOS
[8]	N-path Filter	0.1 ~ 12	1	150	1 ~ 80	3.9 ~ 8.3 ^e	-3.6 ^c @12 GHz	-	~ 20 @12 GHz	130 @12 GHz	0.36	32 nm SOI CMOS
[10]	N-path RX	0.7 ~ 2.5	3 (intra-band)	1 ~ 30	-	4.8	< -19 ^c	< 150	> 40 with a notch	150 ~ 362 ^(b)	7.8	65 nm CMOS
[11]	N-path RX	0.5 ~ 3.6	4 (inter, intraband)	-	-	3.7 ~ 4.5	-7.1 ^c	-	44	46	0.3	28 nm CMOS
[12]	N-path Image-Reject RX	0.5 ~ 3	2 (intra-band)	-	-	4.5	-4.1 ^c	~ 165	25	15 @ 2 GHz	0.16	45 nm CMOS

^aCalculated from $174 + IP_{-1dB} - NF$.

^bIncluding CLK generator power.

^cCalculated from IIP3 - 9.6 dB.

^dAt 9.7 GHz for $Q=20 \sim 50$.

^eInsertion loss+0.9 dB (theoretical minimum NF for 4-pth filter [14]).

Table 2. Performance comparison with off-chip filters

References	Type	No of. Bands	Center Frequencies (GHz)	Ratio of Center Frequencies	BW of each Band (MHz)	In-between bands Attenuation (dB)	Ultimate Rejection (dB)	Area
This Work	Q-enhanced LC on-Chip	2	9.7/13.9 Tunable	1.43	200/200 Tunable	~ 22	> 50	0.37 mm ²
[1]	SIW cavities	2	2.51/5.30	2.11	170/307	~ 31	> 45	-
[4]	Substrate step-impedance resonators	2	1.57/3.5	2.23	240/400	~ 35	> 50	> 300 mm ²
[6]	Folded SIW cavities	2	2.4/5.2	2.17	180/300	~ 33	> 40	-
[7]	SIW cavities	2	9.23/14.05	1.52	260/780	~ 35	> 50	~ 40 cm ²

References

- Li M, Chen C and Chen W (2017) Miniaturized dual-band filter using dual-capacitively loaded SIW cavities. *IEEE Microwave and Wireless Components Letters* **27**, 344–346.
- Psychogiou D, Gómez-García R, Guyette AC and Peroulis D (2016) Reconfigurable single/multi-band filtering power divider based on quasi-bandpass sections. *IEEE Microwave and Wireless Components Letters* **26**, 684–686.
- Liu X, Katehi LPB and Peroulis D (2010) Novel dual-band microwave filter using dual-capacitively-loaded cavity resonators. *IEEE Microwave and Wireless Components Letters* **20**, 610–612.
- Lu Di, Barker NS and Tang X-H (2017) Miniaturized dual-band filter with return loss bandwidth and transmission zero control. *International Journal of Microwave and Wireless Technologies*, **1**, 1–7.
- Sánchez-Renedo M and Gómez-García R (2009) Microwave Dual-Band Bandpass Planar Filter Using Double-Coupled Resonating Feeding Sections, 11th European Microwave Conference Rome, Italy.
- Shen W, Yin W-Y and Sun X-W (2011) Miniaturized dual-band substrate integrated waveguide filter with controllable bandwidths. *IEEE Microwave and Wireless Components Letters* **21**, 418–420.
- Shen Y, Wang H, Kang W and Wu W (2015) Dual-band SIW differential bandpass filter with improved common-mode suppression. *IEEE Microwave and Wireless Components Letters* **25**, 100–102.
- Kibaroglu K and Rebeiz GM (2016) An N-Path Bandpass Filter with a Tuning Range of 0.1–12 GHz and Stopband Rejection \geq 20 dB in 32 nm SOI CMOS, IEEE MTT-S International Microwave Symposium, San Francisco, USA.
- Mohammadi L and Koh K-J (2015) 2–4 GHz Q-tunable LC bandpass filter with 172-dBHz peak dynamic range, resilient to +15-dBm out-of-band blocker, IEEE Custom Integrated Circuits Conference, San Jose, USA.
- Chen R and Hashemi H (2015) Reconfigurable receiver with radio-frequency current-mode complex signal processing supporting carrier aggregation. *IEEE Journal of Solid-State Circuits* **50**, 3032–3046.
- Lee S, Jeong D, Jin H and Kim B (2016) Reconfigurable 4 channel carrier Aggregation Receiver using Harmonic Recombination Technique, 11th European Microwave Integrated Circuits Conference, London, United Kingdom.
- Hwu S-C and Razavi B (2015) An RF receiver for Intra-band carrier aggregation. *IEEE J. Solid-State Circuits*, **50**, 946–961.
- Amin F, Raman S and Koh K-J (2016) A High Dynamic Range 4th-order 4-8 GHz Q-enhanced LC Band-pass Filter with 2-25% Tunable Fractional Bandwidth, IEEE MTT-S International Microwave Symposium, San Francisco, USA.
- Cook BW, Berny A, Molnar S, Lanzisera S and Pister KSJ (2006) Low-power 2.4-GHz transceiver with passive RX Front-End and 400-mV supply. *IEEE Journal of Solid-State Circuits* **41**, 2757–2766.



Farooq Amin received his B.S. degree in computer engineering from COMSATS IIT, Pakistan, in 2005. He received his M.S. degree in electrical engineering with specialization in system-on-chip from Linköping University, Linköping, Sweden in 2009 and the Ph.D. degree in electrical engineering from Virginia Polytechnic Institute and State University, Blacksburg, VA, USA in 2017.

From 2011 to 2013, he was with the CPU design group at Intel Corp. Hillsboro, OR, USA as a Design Engineer working on Intel Hasewell and Broadwell family of microprocessors design. He is currently working for Northrop Grumman Corp. USA as a RFIC Design Engineer. His research interests include RF and mm-wave circuits, analog X-ray read-out circuits and systems, and low-power high speed custom datapath design.

Dr. Amin was the recipient of the IEEE MTT-S International Microwave Symposium Best Student Paper Award (First Place) in 2016. He is also the recipient of Virginia Space Grant Consortium (VSGC) Graduate Fellowship for the years 2015–2017.



Sanjay Raman was born in Nottingham, U.K., on April 25, 1966. He received the B.S. degree (with highest honor) from the Georgia Institute of Technology, Atlanta, in 1987, and the M.S. and Ph.D. degrees from The University of Michigan at Ann Arbor, in 1993 and 1998, respectively, all in electrical engineering. From 1987 to 1992, he was a Nuclear Trained Submarine Officer with the US Navy. In January 1998, he joined the faculty of the Bradley Department of Electrical and Computer Engineering, Virginia Polytechnic Institute and State University, Blacksburg, where he is currently a Professor. He is also currently serving as Associate Vice President, Virginia Tech National Capital Region, where he is responsible for planning and executing region-wide initiatives to enhance the university's research, education, and outreach missions. He is also a founding member of the VT Multifunctional Integrated Circuits and Systems (MICS) research group. His research interests include RF/microwave/millimeter-wave integrated circuits and antennas, high-speed/mixed-signal ICs, interconnects and packaging, RF microelectromechanical/nanoelectromechanical (MEMS/NEMS) devices, and integrated wireless communications and sensor microsystems.

From 2007 to 2013 he served as a Program Manager with the Microsystems Technology Office, Defense Advanced Research Projects Agency (DARPA), Arlington, VA, responsible for major R&D programs in the areas of adaptive RF/mixed-signal integrated circuits, RF MEMS, and 3D/heterogeneous integration technologies.

Dr. Raman has served as an associate editor for the IEEE TRANSACTIONS ON MICROWAVE THEORY AND TECHNIQUES, and on the Technical Program Committee of the IEEE Radio Frequency Integrated Circuits Symposium. He served as Technical Program Co-Chair for the 2014 International Microwave Symposium. He is an Elected Member of the IEEE Microwave Theory and Techniques Society (MTT-S) Administrative Committee.

He was the recipient of the 2007 Virginia Tech College of Engineering Faculty Fellow, the 2000 Presidential Early Career Award for Scientists and Engineers (PECASE) (1999 NSF CAREER Award), the Virginia Tech College of Engineering Outstanding New Assistant Professor Award (2000), and a 1996–1997 Armed Forces Communications and Electronics Association (AFCEA) Postgraduate Fellowship. In 2013 he was awarded the Secretary of Defense Medal for Exceptional Public Service for his service at DARPA.



Kwang-Jin Koh received his Ph.D. degree in electrical and computer engineering from the University of California, San Diego in 2008. For his doctoral study, Dr. Koh developed X-band and Q-band silicon phased arrays which were reported to the US DoD by the DARPA as one of the agency's major achievements in 2007–2008 and successfully found their ways into the active protection systems of

the US aerospace and defense companies.

After several years stint in the semiconductor industry as an engineering researcher at the Electronics and Telecommunications Research Institute (ETRI, Korea) from 2000 to 2004, as a senior engineer at Intel Corp. from 2008 to 2010, and as a senior staff scientist at Broadcom Corp. from 2010 to 2011, he joined in the Virginia Tech ECE Department as an assistant professor and started teaching from the 2012 Spring semester. Dr. Koh's research interests include low-power and power-efficient integrated circuits and systems up to millimeter-wave frequencies.

Dr. Koh and his students received the first place best student paper award in the 2016 IEEE International Microwave Symposium (IMS) and the second place best student paper award in the 2015 IMS. Dr. Koh was also nominated for the R.W.P. King best paper award from the IEEE Antenna and Propagation Society in 2015. Dr. Koh was the recipient of a best paper award of the IEEE Solid-State Circuits and Electron Device Societies, Seoul Chapter in 2002. He and his Ph.D. student also received the 2015–2017 NASA Virginia Space Grant Consortium STEM research fellowship. Dr. Koh received the 2014 Outstanding Assistant Professor Award and the 2012 Junior Faculty Research Award from the College of Engineering, Virginia Tech, and the 2010 Team of the Year Award from Teledyne Technology Inc. (formerly, Teledyne Scientific Corp.). Dr. Koh has been serving as a technical program committee member of the IEEE Bipolar/BiCMOS Circuits and Technology Meeting and IEEE Custom Integrated Circuits Conference.